



OPEN ***P53* status, and G2/M cell cycle arrest, are determining factors in cell-death induction mediated by ELF-EMF in glioblastoma**

Romina Mehdizadeh², Alireza Madjid Ansari¹, Flora Forouzes², Fatemeh Shahriari⁴, Seyed Peyman Shariatpanahi³, Ali Salaritabar¹ & Mohammad Amin Javidi^{1,2}✉

The average survival of patients with glioblastoma is 12–15 months. Therefore, finding a new treatment method is important, especially in cases that show resistance to treatment. Extremely low-frequency electromagnetic fields (ELF-EMF) have characteristics and capabilities that can be proposed as a new cancer treatment method with low side effects. This research examines the antitumor effect of ELF-EMF on U87 and U251 glioblastoma cell lines. Flowcytometry determined the viability/apoptosis and distribution of cells in different phases of the cell cycle. The size of cells was assessed by TEM. Important cell cycle regulation genes mRNA expression levels were investigated by real-time PCR. ELF-EMF induced apoptosis in U87 cells much more than U251 (15% against 2.43%) and increased G2/M cell population in U87 (2.56%, *p* value < 0.05), and S phase in U251 (2.4%) (data are normalized to their sham exposure). The size of U87 cells increased significantly after ELF-EMF exposure (overexpressing *P53* in U251 cells increased the apoptosis induction by ELF-EMF). The expression level of *P53*, *P21*, and *MDM2* increased and *CCNB1* decreased in U87. Among the studied genes, *MCM6* expression decreased in U251. Increasing expression of *P53*, *P21* and decreasing *CCNB1*, induction of cell G2/M cycle arrest, and consequently increase in the cell size can be suggested as one of the main mechanisms of apoptosis induction by ELF-EMF; furthermore, our results demonstrate the possible footprint of *P53* in the apoptosis induction by ELF-EMF, as U87 carry the wild type of *P53* and U251 has the mutated form of this gene.

Brain tumors are among the most fatal form of cancers^{1,2}. There are different categories applied to these tumors according to the histological characteristics, cellular origin (primary brain tumors and secondary brain tumors³), shape, and related tissue⁴. WHO divides brain tumors into two main categories; benign tumors and malignant tumors. Benign tumors which may called low-grade (grade I and II) are non-cancerous, non-aggressive, and have a slow progression rate; whereas, malignant tumors are considered as high-grade (grade III and IV), either the primary ones (originated from the brain tissue) or secondary ones (spread to the brain from elsewhere due to the metastasis) are aggressive, have a rapid progression rate, and tend to metastasis to other organs in the body¹. According to the WHO classification with the concept of histological features, the majority of primary brain tumors belong to the neuroepithelial, such as Gliomas⁵. Gliomas are the most common malignant tumors of the central nervous system (CNS) that arise from the glial cells. Glioblastoma multiforme (GBM) belongs to the grade IV gliomas and is the most aggressive type of brain tumor. Unfortunately, the GBM is one of the most poor-prognosis cancers, even with the advances and aid of the treatments approaches like surgery, chemotherapy, and radiation therapy⁶.

Electromagnetic fields (EMFs) are a group of radiations that can be produced by electrical currents in human-made devices or natural sources. EMFs are divided into two main groups: non-ionizing and ionizing. EMFs are also categorized based on their frequency or wavelength (the radiation energy is directly proportional to the

¹Department of Integrative Oncology, Breast Cancer Research Center, Motamed Cancer Institute, ACECR, Tehran, Iran. ²Department of Genetics, Faculty of Advanced Science and Technology, Tehran Medical Sciences, Islamic Azad University, Tehran, Iran. ³Institute of Biochemistry and Biophysics, University of Tehran, Tehran, Iran. ⁴Department of Molecular Genetics, Faculty of Biological Sciences, Tarbiat Modares University, Tehran, Iran. ✉email: Javidi@acecr.ac.ir

frequency; in the non-ionizing part, the radiation energy is too weak to break chemical bonds, on the other hand, ionizing fields have high energy and can break chemical bonds⁷).

Amounting of studies have reported the anti-cancer effects of the extremely low-frequency EMFs (ELF-EMFs) (0–300 Hz) against various cancers. Many pieces of research performed till now trying to shed light on the underlying molecular mechanism of action of these fields; exposure time, frequency, intensity, and cell type seem to be some important factors in exerting this anti-cancer effect; however, the exact mechanism seems no to be sufficiently transparent yet⁸. One of the main mechanisms which are proposed to the sibling of these fields (electrical fields, renowned as tumor treating field (TTF), which has FDA approval for use in recurrent or early diagnosed GBM patients) is through hindering the mitotic microtubules fibers, inducing the cell cycle arrest in the metaphase and regarding cell to the apoptosis⁶.

Magnetic fields, have some benefits over electrical fields, including higher permeability; this is more crucial when we realize that, the obstructing physical properties including the higher resistance are high in the organs like the head (about 50 Ω in the scalp, skull, and gray matter together⁹). The main aim of this study was to investigate the anti-tumor effect and plausible cellular/molecular mechanism of action of ELF-EMF on two human glioblastoma cell lines U87 and U251 with distinct genetic patterns, specifically according to their *P53* status (U87 has the wild type of this gatekeeper gene, but U251 has mutated form¹⁰).

Materials and methods

Cell culture. Human U87 and U251 MG glioblastoma cell lines and normal human fibroblast (purchased from Pasteur institute of Iran) were cultured in a 25 cm² flask (Nunc, Thermo Fisher) in h-DMEM (High-glucose Dulbecco's modified Eagle's medium) with 10% FBS, 1% penicillin and streptomycin (all from Gibco, Thermo Fisher, USA) at 37 °C in a humidified atmosphere of 5% CO₂ in the incubator (Mettler, Germany). The medium was replaced with a fresh complete medium every 4 days. When cells reached around 80% confluence, they were trypsinized, counted, and then seeded in each well of 6-well plates with a density of 5×10^4 . We further extended the experiments on the MCF-7 cell line to assess how wild-type *P53* status in these cells may be effective in the apoptosis induced by ELF-EMF (the culturing and exposure conditions of these cells were the same as the previous ones).

ELF exposure characteristics. The ELF-EMF exposure device (Parto Farazane Farda, Iran) consists of two pairs of square coils which were manufactured in a U-shape solenoid-like configuration, with an iron core to ensure maximal homogeneity and arise levels of B-field. The coils were wrapped with 1250 single-strand copper wires¹¹. The exposure site dimensions are a 15 × 15 × 15 cm box. A waveform generator (GWInstek SFG-1000 series, South Korea) was linked to the coils for obtaining a magnetic field that could be calibrated between 1–100 mT and 1 to 60 Hz respectively¹² (as described before¹¹) (Fig. 1). U87, U251, and fibroblast cells were exposed to ELF-EMF with the frequency of 1 Hz, and 100 mT intensity, for 5 days, 2 h each day. Sham exposure as the control of this study had the same condition as the exposed groups but the generator set is off. So, the field condition at the sham exposed group was equal to the background level (around 110 μ T). All of the area related to the exposure site has been thoroughly calibrated by using the Lakeshore® Gauss meter on a net-like plastic plate situated at bottom of the exposure place. Following calibration, an 8 × 8 cm square at the middle of the exposure site, in which the field fluctuation is less than 2%, was considered an exposure area. Also, a cold air conditioner has

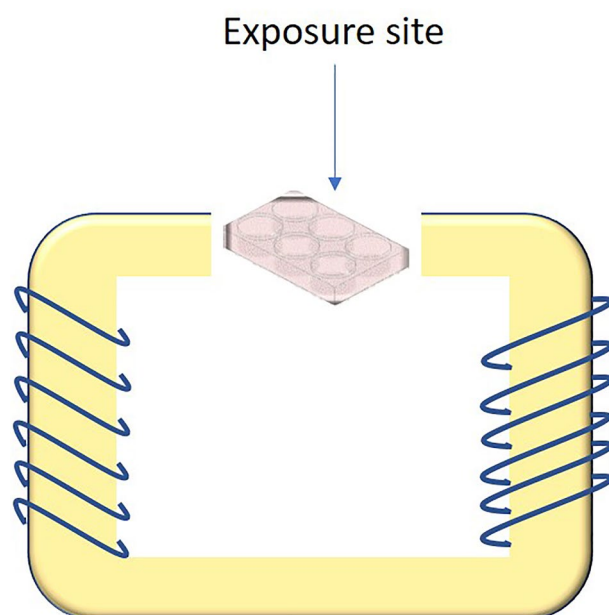


Figure 1. ELF-EMF schematic view and the exposure site.

been situated near the iron core and coils to reduce probable overheat. Although the temperature setting would not exceed the maximum 37° C based on the thermodynamic predictions, the cold air current would guarantee the temperature stabilizing during the field generation.

Cell proliferation assay. All three cell lines were seeded, at a density of 0.5×10^5 cells/ml in DMEM medium. After 5 days, exposed and sham exposed groups cells were harvested, washed, and re-suspended in 0.4% trypan blue in PBS solution. The number of viable cells was counted using Neubauer lam according to standard protocol (the cells which stained blue was considered dead cells and those that didn't stain were considered live cells).

Overexpressing P53. To assess the P53 role in apoptosis induction by ELF-EMF, pCMV-Neo-Bam-H1-p53 plasmid was used. This plasmid was kindly provided by Dr. Michael Resnick (NIEHS, NIH), by the aid of BamHI restriction enzyme and cloning, cDNA of P53 was inserted into the pCMV-NeoBam vector from Addgene (Cambridge, Massachusetts, USA) (reference¹³ shows the vector map). U251 cells were transfected with 100 ng/μl concentration of this plasmid (abbreviated as U251-P53), by Lipofectamine®2000.

Flow cytometry. After 5 days of ELF exposure, U87 and U251 MG glioblastoma and fibroblast exposed and sham exposure both were collected by trypsinizing and centrifugation at 1200 rpm (Sigma, USA) to reach cell pellets. The pellets were then re-suspended in PBS (phosphate buffered saline, Gibco, USA), and utilized as the template for the flow cytometry test (BD FACSCalibur™). To assess the kind of cell death Annexin V/PI, (eBio-sciencesDx) (the Annexin V-FITC IQ products, Netherlands) (20 and 5 μl, respectively) corresponding signal provides a very sensitive method for detecting cellular apoptosis, while propidium iodide (PI) (2 μl) (Sigma-Aldrich, Germany) is used to detect necrotic or late apoptotic cells, characterized by the loss of the integrity of the plasma and nuclear membranes) performed. We further investigated the cell cycle distribution of cells by determining the cellular DNA content with a saturating amount of DNA-binding dye. After 5 days of exposure to ELF-EMF, exposed and sham exposure cells were collected. These cells were washed twice with PBS and incubated with propidium iodide (10 μg/ml) and RNase A (0.1 mg/ml) (Sigma-Aldrich, Germany) for 30 min at 37 °C and then the distribution of cells in the different cell cycle phases was analyzed by Flow cytometer using FlowJo software v 10.2.

Real-time PCR. Alteration in the mRNA expression level of *P21*, *P53*, *MDM2*, *MCM6*, and *CCNB1* in U87 and U251 cells after exposure was determined by using real-time PCR. Total RNA was extracted by using the TRIzol reagent (Invitrogen). Reverse transcription on the extracted RNAs was performed by using the Revert Aid First Strand cDNA Synthesis Kit (Thermo Fisher). These cDNAs were subsequently used as the template for real-time PCR. Primers were designed by using NCBI primer design software (Table1) (*Gapdh* used as house-keeping/internal control) to specifically amplify cDNAs of the mentioned genes. The real-time PCR reaction was performed on StepOnePlus™ real-time PCR device (Applied Biosystems, USA) in 96-well microtiter plates by using the SYBR Green PCR Master Mix (AMPLIQON, Denmark). The thermal cycling of stages consisted of an initial denaturation step at 95 °C for 15 min, 40 cycles at 95 °C for the 20 s, and 60 °C for 1 min, followed by a melt curve step.

Transition electron microscopy (TEM). After 5 days of treatment by ELF-EMF, U87, U251, and fibroblast cells were collected by trypsinizing and centrifuged at 1200 rpm. Transmission electron micrograph (TEM) images were recorded from the Pasteur Institute of Iran. For TEM analysis, the sample particles were dispersed in ethanol and then dropped onto copper grids with porous carbon films.

Statistical analysis. The obtained data were evaluated by GraphPad prism8. The total of the study was measured as mean ± standard deviation (SD). For comparison between the two groups the t-test was applied, in cases where another statistic test has been applied, it is mentioned accordingly. Statistical significance was expressed as a *p-value* < 0.05.

Gene name	Accession number	Primers Sequence (5' to 3')	Amplicon length(bp)
<i>P53</i>	NM-000546	F: TGTGACTTGCACGTA CTCCC R: ACCATCGCTATCTGAGCAGC	199
<i>P21</i>	NM-000389	F: GACCATGTGGACCTGTCACT R: CGTTTGGAGTGGTAGAAATCTGTGTC	140
<i>MDM2</i>	NM-001145337	F: TCTGTGAGTGAGAACAGGTGTCTCR: TGGCGTTTTCTTTGTGCTGTCA	191
<i>MCM6</i>	NM-005915	F: CAGCATTAAAGAGGAGCGAGC R: GCTCTCACTTCCCTCTGTGG	191
<i>CCNB1</i>	NM-001354844	F: GCACTTCCTTCGGAGAGCAT R: TGTCTTGACAGTCCATTCACCA	188

Table 1. Primers sequence used for real-time PCR.

Results

Cellular morphology changes. *Optical microscope analysis.* Morphological changes after exposure were determined in two groups (sham exposure and exposed) of all cells, firstly by an inverted optical microscope (Olympus). As shown in Fig. 2, after 2 h/day exposure to ELF-EMF, exposed U87, U251, and U251-P53 cell lines underwent morphological alteration concerning the shape and the size of the cells. The morphological analysis demonstrated that the shape of exposed U87, U251, and U251-P53 cell lines changed to a spherical shape on the fifth day. Whereas, in normal fibroblast cells there were no significant differences in exposed and sham exposure. Moreover, a reduction in the cell population on the fifth day was observed in exposed U87 cells. The trypan blue results demonstrated that after exposure the rate of proliferation decreased significantly in all cells after the fifth day of exposure compared with the unexposed cells (the sham exposure); although this decrease was not statistically significant in the U251-P53 group (p value = 0.0849) (Fig. 2).

Annexin V/PI. Apoptosis assay was performed by the double staining method (Annexin V-FITC/PI kit) and the percentage of dead cells, early apoptosis, late apoptosis, and live cells were assessed by flow cytometry. Flow cytometry analysis showed that the percentage of apoptosis (early + late apoptotic cells), cell death, and necrosis were respectively in U87 (11.39%, 15.45%, and 3.64), U251 (2.43%, 4.55% and 2.04%), U251-P53 (8.15%, 10.7%, and 3.35%), MCF-7 (13.15%, 16.8%, and 4.85%), and Fibroblast (2.19%, 0.95% and -1.18%). All the results were represented as the difference between the exposed groups and the corresponding sham exposure. Apoptosis rate increased significantly in U87 and U251 cell lines post-exposure; however, there were no differences in normal fibroblast. When comparing the two GBM cell lines, it was ascertained that ELF-EMF exposure could significantly increase the apoptosis rate in U87 compared to U251 (Fig. 3).

Cell cycle. To evaluate the effect of ELF-EMF on the distribution of cells in different cell cycle phases, flow cytometry was performed. As shown in Fig. 4, ELF-EMF exposure led to a significant increase in the accumulation of cells at the G2/M phase (2.56%) in the U87 cell line; whilst the other two cell lines didn't show/show negligible distribution changes in this phase. In the case of the U251 cell line, a trivial increase in the S phase was observed (2.4%) in the exposed cells compared with its sham exposure. Furthermore, in the fibroblast cell line, ELF-EMF exposure led to an insignificant increase in cell distribution at the subG1 phase (4.88%). Interestingly,

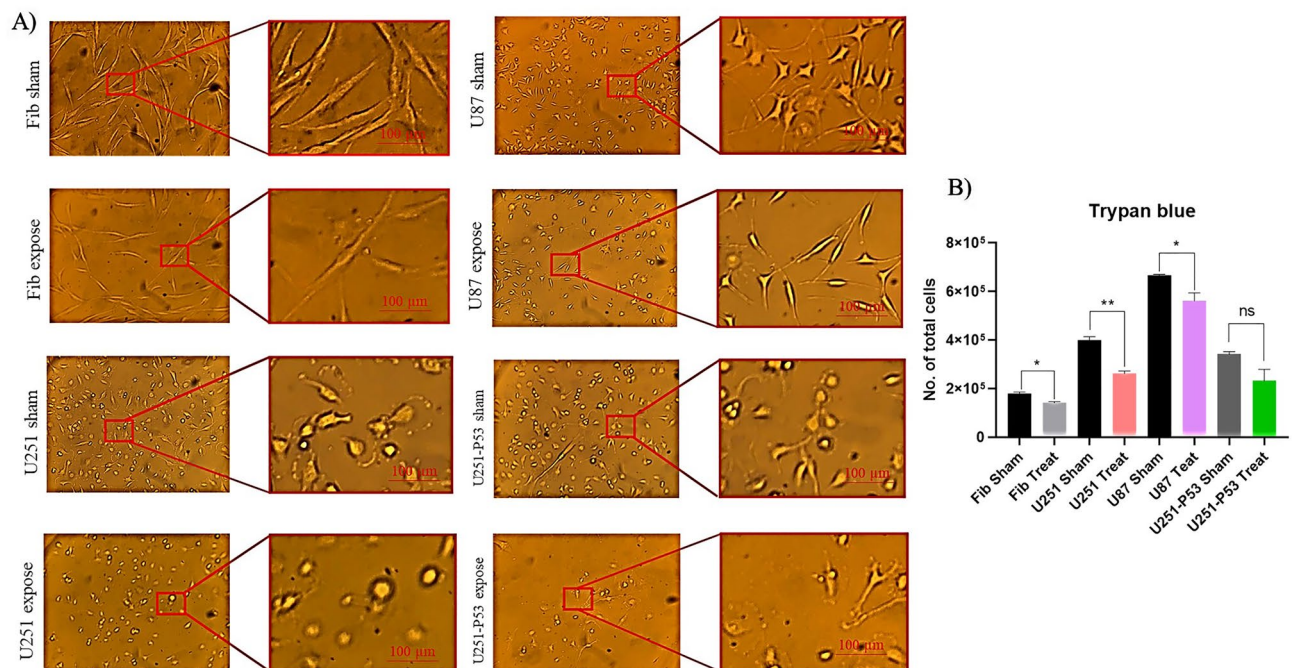


Figure 2. Cellular morphology and proliferation alteration under light microscope before and after ELF-EMF exposure. (A) After five days, the shape of cancerous cells which were exposed to the ELF-EMF altered and the rate of rounded cells (which may be interpreted as cells undergo apoptosis) was much more in them (fifth day, exposed U87 and U251); these shapes were rare in the fibroblasts. Comparing the two cancerous cells, the rate of rounded cells was much more in U87, furthermore, it seemed that cancerous cells weren't able to proliferate as much as their sham exposure group. (B) Trypan blue results for the fifth day revealed that after exposure the total number of cells in the exposed groups is less compared with their corresponding sham exposure (the same number of cells were seeded for each exposed and sham exposure group (the first day: just before exposure)). This decrease was statistically significant in fibroblast, U251, and U87 cells (*: p -value < 0.05; **: p -value < 0.01); however, in the U251-P53 group this increase was not statistically significant (Mann–Whitney U test performed as statistical analysis to compare each exposed group with its sham exposure).

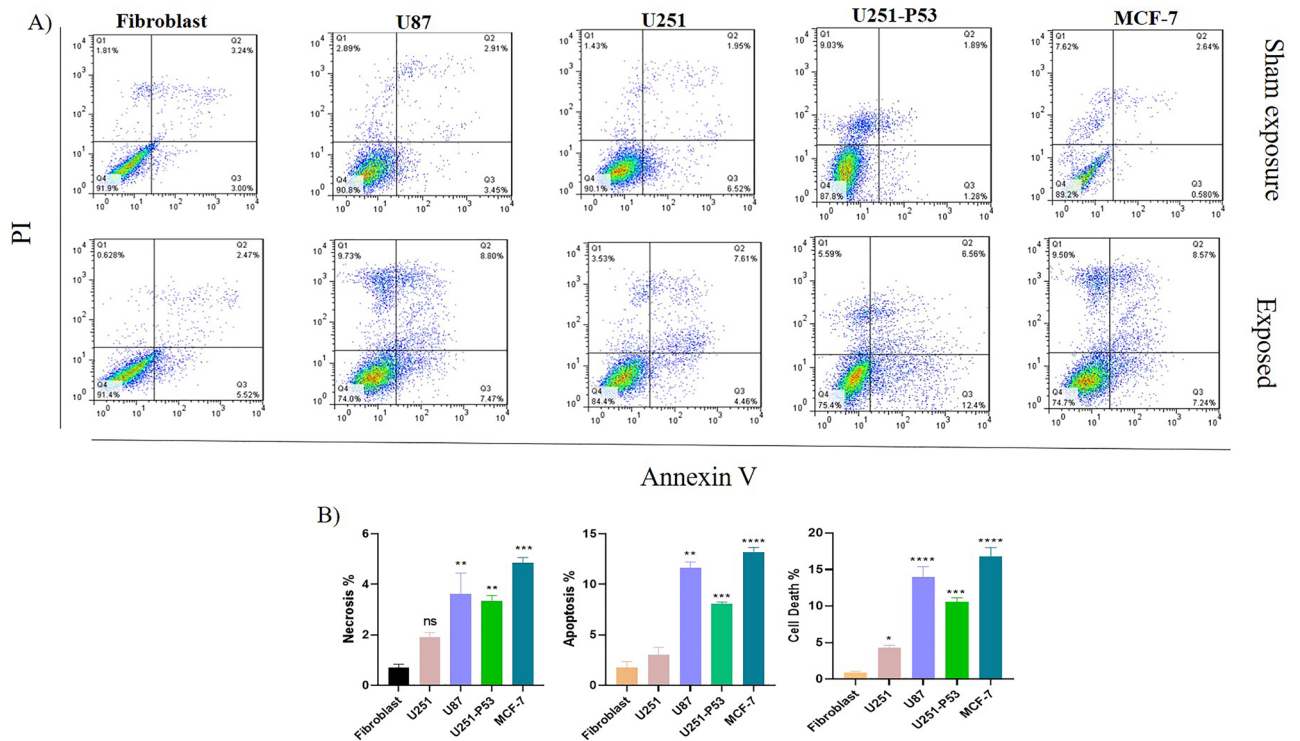


Figure 3. (A) Flow cytometry histogram showed the changes in the percentage rate of necrosis (Q1: PI+/AnnexinV−), late apoptosis (Q2: PI+/AnnexinV+), early apoptosis (Q3: PI−/AnnexinV+) and live cells (Q4: PI−/AnnexinV−). The percentage of live cells decreased significantly in U87, U251-P53, and MCF-7 compared to Fibroblast. (B) Flow cytometry diagram of 5 groups fibroblast, U251, U87, U251-P53, and MCF-7. This graph is normalized using sham exposure groups. Respectively, necrosis, apoptosis, and cell death rate in fibroblasts were calculated to be about 1.18%, 2.19%, and 0.95%, in U251 2.04%, 2.43%, and 4.55%, in U87 3.64%, 15%, and 11.28%, in U251-P53 3%, 8%, and 11.2%, and in MCF-7 5%, 13%, and 17.9%. According to the graphs, a significant increase in apoptosis and cell death was observed in the U87, U251-P53, and MCF-7 cell line compared to the fibroblast (**p*-value < 0.05, ***p*-value < 0.01, ****p*-value < 0.001, *****p*-value < 0.0001). The experiments were performed twice for each cell line under the exposure. (The place of quadrants was normalized according to the sham exposure and the control group; the differences between exposed (exposed to ELF-EMF with 1 Hz, 100 mT, 2 h each day for 5 days) and sham exposure groups used to report the apoptosis, necrosis, and cell death; one-way ANOVA was applied).

in the case of U251-P53 cells, after exposure, the frequency of cells in the sub-G1 and G2/M phases increased (0.92, and 1.1% respectively), and the distribution of cells in the S phase decreased (Fig. 4, and Table 2).

Real-time PCR. To verify the effect ELF-EMF on the important genes' expression involved in the cell cycle progression and/or apoptosis, alteration in the expression level of five genes (*P21*, *P53*, *MDM2*, *MCM6*, and *CCNB1*) was assessed by qRT-PCR. According to the real-time PCR data, the mRNAs expression level of *P21*, *P53*, and *MDM2* were increased in the exposed group of U87 cells compared to the sham exposure (about 2.5, 14, and 1.8-fold more, respectively). While the expression level of *CCNB1* was decreased following ELF-EMF exposure in these cells. The mRNA expression level of *P21*, *P53*, and *MCM6* down-regulated in U251 cells after exposure. The expression level of *P21* and *P53* increased in the U251-P53 and fibroblast cell lines after exposure (for *P21* 1.6 and fivefold more; for *P53* 3.6, and 4.65-fold more, respectively in U251-P53 and fibroblast). When comparing the expression level of the mentioned genes between these two cell lines, we realize that the expression level of *P53* increased and *CCNB1* decreased much more, after exposure, in the U87 cells than in the U251 cells (Fig. 5).

Transition electron microscopy (TEM). To further assess the impact of ELF-EMF exposure on the cells' shape and size, transmission electron microscopy (TEM) was performed. Results demonstrated slight changes in the cell size of the fibroblast and U251 cells compared with their corresponding sham exposure. This alteration was significantly more in the U87 cells (about 1.7-fold more compared with its sham exposure, *p* value = 0.0231). U251-P53 and MCF-7 cells' size increased about 1.06, and 1.2-fold after exposure; however, this increase was not statistically significant (*p* value > 0.05) (Fig. 6).

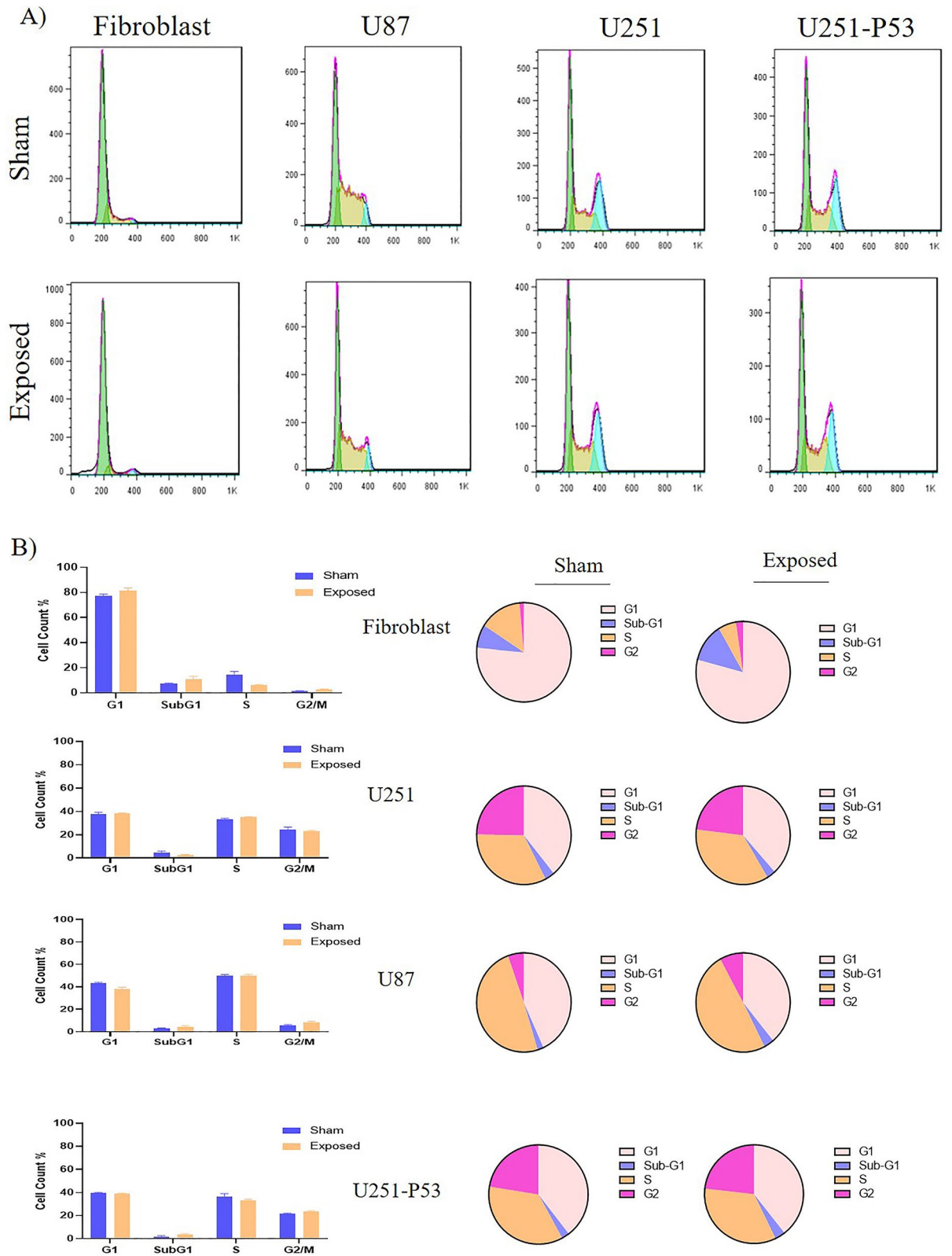


Figure 4. (A) Flow cytometry histogram showed alteration in the distribution of cells in different phases of the cell cycle in exposed (exposed to ELF-EMF with 1 Hz, 100 mT, 2 h each day for 5 days) and sham exposure groups of different cell lines. (B) Column (left) and pie chart (right) diagrams of flow cytometry results for the cell cycle. Respectively, subG1, G1, S, and G2/M phases distribution of cells in fibroblasts were 4.88%, 2.66%, – 8.43%, and 0.99%, in U251 were – 0.3%, – 1.1%, 2.4%, and – 1.79%, and (there was a slight increase in S phase), in U87 calculated to be 1.43%, – 4.6%, – 0.18%, and 2.56% (increased rate in G2/M phase), and in U251-P53 0.92, 0.28%, – 1.16%, and 1.1% (a slight increase in G1 and G2/M phases and slight decrease in S phase) (the minus results represent decreasing and the positive results are representative of increasing in the rate) (this result obtained from two independent experiments). (The frequency of cell distribution in each phase of the cell cycle was compared between the sham exposure and the exposed group by using the Mann–Whitney U test).

Cell line	G1-Freq%	SubG1-Freq%	S-Freq%	G2-Freq%	Apoptosis%
Fibroblast	2.66	4.88	- 8.43	0.99	2.18
U251	- 1.1	- 0.3	2.4	- 1.79	2.47
U87	- 4.6	1.43	- 0.18	2.56	11.39
U251-P53	0.28	0.92	- 1.16	1.1	8

Table 2. Rate of the cells distribution in different cell cycle phases and their relation with percentage of apoptosis. Data represents the results obtained from the exposed cells minus the results of the sham exposure (delta).

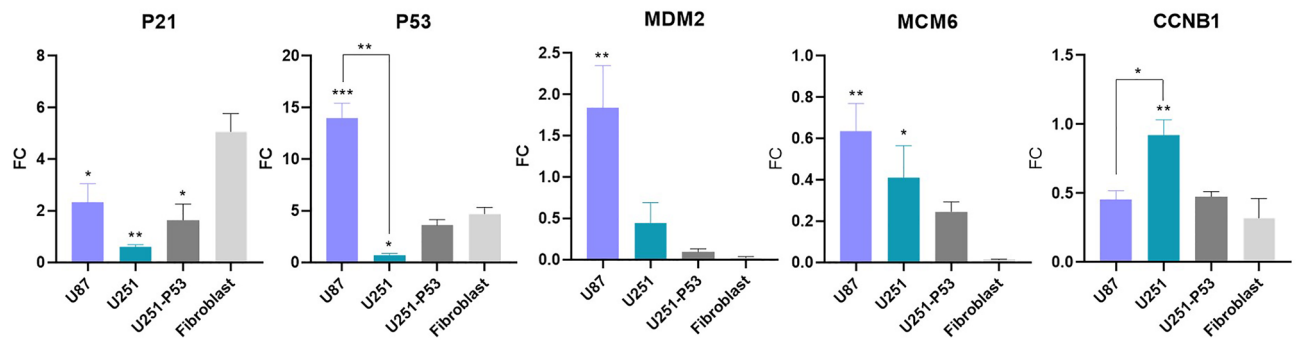


Figure 5. Changes in the mRNA expression level of *P53*, *P21*, *MDM2*, *MCM6*, and *CCNB1* genes in U87 and U251 cell lines after ELF-EMF exposure. The expression level of *P53*, *P21*, and *MDM2* genes increased in U87, U251-P53, and fibroblast cell lines (as data are presented as fold change (FC), the values more than 1 are considered as increasing, and values less than 1 are considered as decreasing). *MCM6* and *CCNB1* decreased in all three mentioned cell lines. In the case of U251, *P53*, *P21*, and *MCM6* were down-regulated after exposure. When comparing the alteration in the expression level of these genes in U87 and U251 cells, it came out that, the *P53* expression level was much lower in the U251 (p value = 0.0057), and *CCNB1* was much higher in U251 (p value = 0.0348) (this result obtained from two independent experiments and one-way ANOVA statistical analysis performed to analyze the results).

Discussion

Apoptosis induction. Glioblastoma is one of the poorest prognosis cancers of primary brain tumors with a high mortality rate and poor prognosis. Current therapy options for glioblastoma include surgery, chemotherapy, and radiotherapy which are prescribed mostly as combination therapy. In this regard, the treatment of glioblastoma is a serious challenge due to the confined number of therapeutic options available^{14–16}. Recently, numerous studies have shown that magnetic field (MF) therapy provides a new safe treatment method with the advantage of high efficiency and low side effects^{17,18}. Low-frequency magnetic fields such as ELF-EMF are reported to have the potential to affect crucial cancer-related biological processes including apoptosis, the regulation of immunity, and suppression of angiogenesis. Moreover, amounting studies have shown that low-frequency magnetic fields could inhibit cancer proliferation and have tumor inhibitory effects; however, the mechanism of this technique remains poorly understood^{19–21}. It is important to mention that ELF-EMF may interfere with some chemotherapeutic interventions; some studies have shown that it may promote the cytotoxicity and on the other hand others have shown that it may play as an inhibitory factor. It seems that the outcome in this area, at least at some steps, is due to the mechanism of action of the ELF-EMF which is related to the reactive oxygen species (ROSs) production. Moreover, these outcomes are strictly dependent to the characteristics of the fields (intensity, frequency, and time of exposure)^{22–26}.

According to the previous study, electric fields such as Tumor Treating Fields (TTFields) exert an anti-cancer effect in a *P53*-dependent manner⁶. Previously, we showed that ELF-EMF has the potential to trigger apoptosis/necroptosis in different breast cancer cells^{27,28}; here, by selecting two different GBM cell lines with different *P53* statuses (U87 and U251), at the first step, we tried to investigate the dependency of ELF-EMF anti-cancer effect on this gene. In the next step, the relation between this exposure, cell cycle progression, and cell size is assessed further at the molecular level. The annexin V/PI flow cytometry results revealed that ELF-EMF induces apoptosis in U87 cells much more than in U251 cells (meager apoptosis was seen in the normal fibroblasts after exposure). As we know *P53* status in U87 is wild-type and in U251 it has the mutation. This result may reflect the possible footprint of this gene in ELF-EMF-dependent apoptosis induction and different cellular response to this exposure (discussed in more detail in the next paragraphs).

Relationship between the examined genes expression and cell cycle arrest. To investigate the impact of ELF-EMF on cell cycle progression, important gene expression in this area (*P21*, *P53*, *MDM2*, *MCM6*,

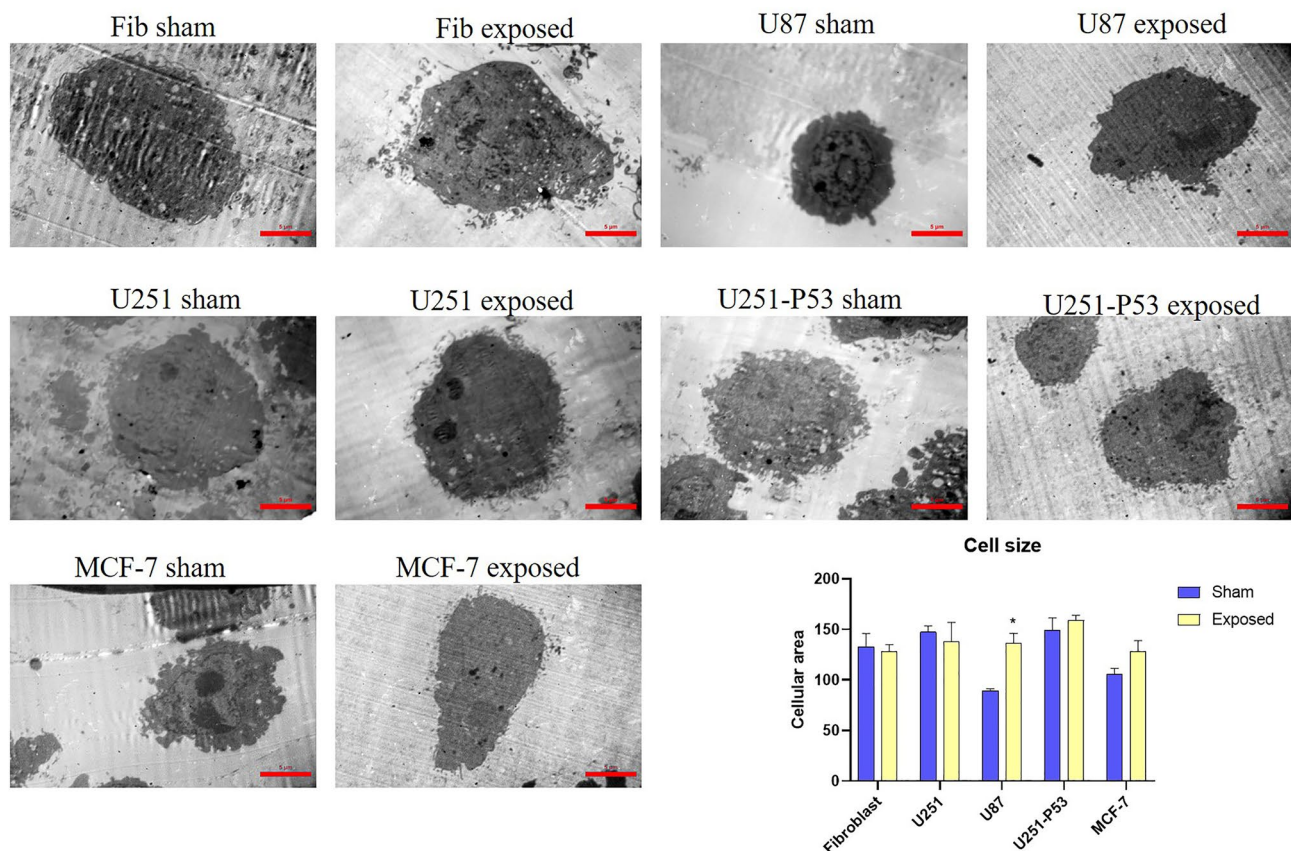


Figure 6. Images obtained from transmission electron microscopy to evaluate alteration in the cell size of U87, U251, U251-P53, MCF-7, and fibroblast cells after exposure to ELF-EMF. Results showed that cell size increased significantly in U87 cells (p value = 0.0231) compared to its sham exposure. While U251 and fibroblast cells didn't show significant changes. U251-P53 and MCF-7 cells showed an increase in their cell size; although this increase was not statistically significant (p value = 0.4132, and, p value = 0.1271, respectively) (Mann-Whitney U test was used to compare cells' size in between two groups (exposed and sham exposure) of each cell line).

and *CCNB1*) was assessed by real-time PCR. Results demonstrated that *P53*, *P21*, and *MDM2* up-regulated in U87, but they showed no significant changes in U251. On the other hand, *MCM6* and *CCNB1* were down-regulated in U251 and U87. *P21* can be directly regulated by the *P53*, and it is not out of mind to expect their expression pattern to act similarly; moreover, *P21* can induce apoptosis and cell cycle arrest in the G1/S and G2/M phase of the cell cycle^{29,30} (these are following the data obtained from annexin V/PI and cell cycle flow cytometry). *MDM2* (mouse double minute 2) is a negative regulator of *P53*; *MDM2* regulates the *P53* level and its activity^{31,32}. Our results revealed that the *MDM2* expression level increased in the U87 cell line; although we expect the latter increase to exert a negative effect on the *P53* expression/function, as the expression level of *P21* increased, we may conclude that *MDM2* didn't succeed to exert its negative regulation on the *P53*. This may be at least in some steps, due to the increase in *MDM2* was not enough to overcome and block the *P53* increase (*P53* expression level increased much more in the U87 cells compared with *MDM2* increasing).

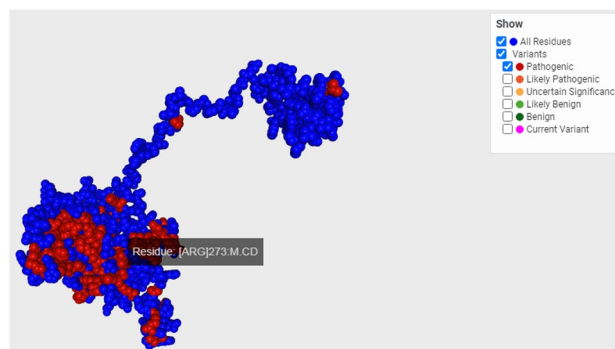
In the case of U251, the expression level of *CCNB1* and *MCM6* decreased in this cell line after exposure. *MCM6* is a member of the mini-chromosome maintenance family (MCM), which plays an important role in limiting the replication in each cell cycle³³. *MCM6* has helicase activity which leads to the recruitment of DNA polymerase and the initiation of DNA replication³⁴. *MCM6* is a candidate marker for cell proliferation; an increase in *MCM6* levels indicates the proliferation of malignant cells. Overexpression of *MCM6* is found in many human cancers, and knocking down it significantly inhibits cell proliferation^{35–39}. From a cell cycle point of view, inhibiting *MCM6* can delay the progression of the cell cycle from G1/S by down-regulating the expression of cell cycle checkpoint proteins. This result is following cell cycle flow cytometry data for U251, where a meager increase in the population of cells in the S phase is revealed (Fig. 4B). *CCNB1*, encoded by the *CCNB1* gene, belongs to the cyclin super family⁴⁰. *CCNB1* has a key role in Cdk1 regulation and transition from the G2 phase to mitosis progression⁴¹. *CCNB1* also called cyclin B1, has shown that is closely associated with tumor progression and was highly expressed in tumor tissues or cells⁴². Our results demonstrated that down-regulating of *CCNB1* is more significant in U87 cells than U251; hence, it is not out of mind to expect that the rate of cells in the G2/M phase of the cell cycle shall be more in the exposed U87 cells compared with the U251. Along with the crucial role of this gene in the transition of the cell cycle from G2/M, *CCNB1* down-regulation can also up-regulate *P53*

Genes	Cell cycle arrest	Progression cell cycle
P21	G1/S, G2/M	–
P53	G1/S, G2/M	–
MDM2	–	Negative control of p53
MCM6	Downregulation results in delay in S/G2	G1/S
CCNB1	Downregulation results in G2/M arrest	G2/M

Table 3. Role of P21, P53, MDM2, MCM6, and CCNB1 role in cell cycle arrest/progression.

Cell lines	P53 status	Mutation information			Chromosome position	SNIP RS
		In protein	In cDNA	Exon		
U87	WT	–	–	–	–	–
U251	MT	p.Arg273Leu	c.818G>T	exon 8 of 11 position 36 of 137 (coding)	17p13.1 (7673802)	Rs28934576

Table 4. P53 status in U87 and U251. U87 cell line has wild-type p53, however U251 has the mutated form of this gene. We can see the mutated amino acid location in the protein from protein structure obtained from the PDB.



and subsequently *P21* which in turn leads to cell cycle arrest⁴³. To confirm this, it is important to mention that, Zhang et al. and Li et al. showed that down-regulating *CCNB1* prevents cancer progression through *P53* signaling pathway activation⁴¹ which has a key role in mediating the responses of cancer treatments⁴⁴. Table 3 summarizes the role of the mentioned genes in the progression or inhibition of the cell cycle (Table 3).

P53 status. *TP53* is a major tumor suppressor⁴⁵ that has a central role in various cellular responses including apoptosis⁴⁶, DNA repair⁴⁷, and cell cycle⁴⁸. Amounting of recent studies have shown that not only does *TP53* serve a central role in the regulatory network of tumorigenesis, but also its status is closely associated with the disease progression and survival of patients with GBM during radio/chemo therapy^{49,50}; this gene is also considered as a targeted therapy for cancer treatment⁶. The importance of *P53* in the response to the treatment in GBM patients, on one hand, and on the other hand possible footprint of *P53*-dependent apoptosis induction by the electrical field⁶; by choosing two GBM cell lines with different *P53* status (U87 as wild type and U251 as mutated type (Table 4)), we struggled to assess the possible role of this gene status in the response obtained after ELF-EMF exposure. Apoptosis may be induced by *P53*-dependent or independent pathways. Our results answered some parts of this question, as we can see, the apoptosis rate induced in the U87 cells after ELF-EMF exposure is much more than in the U251 cells. It is shown that overexpression of *P53* in the U87 cell line after exposure may be the main reason for apoptosis induction by radiation^{51,52}, as in the U251 cell line, *P53* is mutated it is not out of mind to expect that the underlying and *P53*-dependent pathways which may result in apoptosis after treatment, do not function correctly¹³. The results obtained for the MCF-7 (with wild type *P53*) or U251-*P53* (U251 cells that received vector overexpressing *P53*) also confirmed the role of this gene in the apoptosis induction by ELF-EMF in GBM cells. As we can see, in MCF-7 cells or after overexpression of *P53* in U251 cells, the apoptosis rate increased in the U251-*P53* cells.

Relationship between G2/M cell cycle arrest and cell size. Our results revealed that after exposure to ELF-EMF, the rate of U87 cells in the G2/M phase of the cell cycle increased (as described earlier can be due to the up-regulation of *P53* and subsequently *P21* in these cells). As we know during the interphase of the cell cycle (G1, S, and G2) cell growth occurs and human cells become tetraploid after the replication in the S phase. Hence, it is not out of mind to say that before the mitosis and cell division (karyokinesis and cytokinesis) the volume of cells is more than those which reside in the early phases of the cell cycle (specifically before the S phase). One of

the main mechanisms which have been proposed for tumor treating field (TTF) to act as an anti-cancer modality, is through affecting the microtubules and actin dynamics. With this point of view, TTFs interfere with the normal formation of the spindle in cell division and arrest cells in the metaphase of mitosis, which can be reflected as G2/M arrest in the cell cycle flow cytometry⁵³. This phenomenon increases the cell size of the treated cells. In addition to G2/M arrest, nuclear size can increase due to cellular stresses such as that caused by reactive oxygen species, senescence, and necrosis⁵⁴. The results obtained from the TEM here revealed that the cell size of the U87 cells, which had G2/M arrest, increased significantly after exposure to the ELF-EMF; the underlying mechanism of action here seems to be the same as the TTF field.

Conclusion

ELF-EMF anti-cancer effect is sensitive to the *P53* status in the exposed cells (U87 cells with wild-type *P53* are more sensitive to this field compared with the U251 which has a mutated form of *P53*). Our results suggest that G2/M arrest and increase in the cell size can be the main mechanism of apoptosis induction by these fields. These three (*P53* status, G2/M arrest, and increase in the cell size) are similar between the ELF-EMF and renowned TTFs, which can be a lantern that helps in reaching ELF-EMF to the bedside, just like its cousin the TTF field.

Data availability

Data will be available on request to the corresponding author (Mohammad Amin Javidi; email: Javidi@acecr.ac.ir).

Received: 12 December 2022; Accepted: 30 June 2023

Published online: 05 July 2023

References

- Mohsen, H., El-Dahshan, E.-S.A., El-Horbaty, E.-S.M. & Salem, A.-B.M. Classification using deep learning neural networks for brain tumors. *Future Comput. Inform. J.* **3**, 68–71 (2018).
- Kavitha, A., Chitra, L. & Kanaga, R. Brain tumor segmentation using genetic algorithm with SVM classifier. *Int. J. Adv. Res. Electr. Electron. Instrum. Eng.* **5**, 1468–1471 (2016).
- Tandel, G. S. *et al.* A review on a deep learning perspective in brain cancer classification. *Cancers* **11**, 111 (2019).
- Ismael, S. A. A., Mohammed, A. & Hefny, H. An enhanced deep learning approach for brain cancer MRI images classification using residual networks. *Artif. Intell. Med.* **102**, 101779 (2020).
- <https://www.aans.org/en/Patients/Neurosurgical-Conditions-and-Treatments/Brain-Tumors>
- Lee, Y.-J. *et al.* Gene expression profiling of glioblastoma cell lines depending on TP53 status after tumor-treating fields (TTFs) treatment. *Sci. Rep.* **10**, 1–14 (2020).
- Feychting, A. A. M. Electromagnetic radiation. *Br. Med. Bull.* **68**, 157–165. <https://doi.org/10.1093/bmb/ldg030> (2003).
- Barati, M. *et al.* Cellular stress response to extremely low-frequency electromagnetic fields (ELF-EMF): An explanation for controversial effects of ELF-EMF on apoptosis. *Cell Prolif.* **54**, e13154 (2021).
- McCann, H., Pisano, G. & Beltrachini, L. Variation in reported human head tissue electrical conductivity values. *Brain Topogr.* **32**, 825–858 (2019).
- Motaln, H. *et al.* Heterogeneous glioblastoma cell cross-talk promotes phenotype alterations and enhanced drug resistance. *Oncotarget* **6**, 40998 (2015).
- Barati, M. *et al.* Necroptosis triggered by ROS accumulation and Ca²⁺ overload, partly explains the inflammatory responses and anti-cancer effects associated with 1Hz, 100 mT ELF-MF in vivo. *Free Radic. Biol. Med.* **169**, 84–98 (2021).
- Ansari, A. M. *et al.* Extremely low frequency magnetic field enhances glucose oxidase expression in *Pichia pastoris* GS115. *Enzyme Microb. Technol.* **98**, 67–75 (2017).
- Abbasy, Z. *et al.* Simultaneous treatment with P53 overexpression and interferon γ exerts a dramatic increase in apoptosis induction of U87 cells. *Galen Med. J.* **10**, e2270–e2270 (2021).
- Diao, W. *et al.* Behaviors of glioblastoma cells in in vitro microenvironments. *Sci. Rep.* **9**, 1–9 (2019).
- Xiao, W., Sohrabi, A. & Seidlits, S. K. Integrating the glioblastoma microenvironment into engineered experimental models. *Future Sci. OA* **3**, FSI189 (2017).
- Gierzyng, A., Pyszczolkowska, D., Walentynowicz, K. A., Rajan, W. D. & Kaminska, B. Immune microenvironment of gliomas. *Lab. Invest.* **97**, 498–518 (2017).
- Barati, M., Fahimi, H., Farahmand, L. & Madjid Ansari, A. 1Hz 100mT electromagnetic field induces apoptosis in breast cancer cells through up-regulation of P38 and P21. *Multidiscip. Cancer Investig.* **4**, 23–29 (2020).
- Xu, A., Wang, Q. & Lin, T. Low-frequency magnetic fields (lf-mfs) inhibit proliferation by triggering apoptosis and altering cell cycle distribution in breast cancer cells. *Int. J. Mol. Sci.* **21**, 2952 (2020).
- Nie, Y. *et al.* Effect of low frequency magnetic fields on melanoma: Tumor inhibition and immune modulation. *BMC Cancer* **13**, 1–11 (2013).
- Filipovic, N. *et al.* Electromagnetic field investigation on different cancer cell lines. *Cancer Cell Int.* **14**, 1–10 (2014).
- Destefanis, M. *et al.* Extremely low frequency electromagnetic fields affect proliferation and mitochondrial activity of human cancer cell lines. *Int. J. Radiat. Biol.* **91**, 964–972 (2015).
- Bektas, H. & Dasdag, S. Extremely low frequency magnetic field alters cytotoxicity of irinotecan in glioblastoma: A preliminary observation. *Dicle Tip Dergisi* **48**, 396–403 (2021).
- Akdag, M. Z., Dasdag, S., Aydin Ketani, M. & Sagsoz, H. Effect of extremely low frequency magnetic fields in safety standards on structure of acidophilic and basophilic cells in anterior pituitary gland of rats: An experimental study. *J. Int. Dent. Med. Res.* **2**, 61–66 (2009).
- Akdag, M. Z. *et al.* Can safe and long-term exposure to extremely low frequency (50 Hz) magnetic fields affect apoptosis, reproduction, and oxidative stress?. *Int. J. Radiat. Biol.* **89**, 1053–1060 (2013).
- Akdag, M. Z. *et al.* Do 100- and 500- μ T ELF magnetic fields alter beta-amyloid protein, protein carbonyl and malondialdehyde in rat brains?. *Electromagn. Biol. Med.* **32**, 363–372 (2013).
- Dasdag, S. *et al.* Role of 2.4 GHz radiofrequency radiation emitted from Wi-Fi on some miRNA and fatty acids composition in brain. *Electromagn. Biol. Med.* **41**, 281–292 (2022).
- Koh, E. K. *et al.* A 60-Hz sinusoidal magnetic field induces apoptosis of prostate cancer cells through reactive oxygen species. *Int. J. Radiat. Biol.* **84**, 945–955 (2008).
- Crocetti, S. *et al.* Low intensity and frequency pulsed electromagnetic fields selectively impair breast cancer cell viability. *PLoS ONE* **8**, e72944 (2013).

29. Ren, J. *et al.* LF-MF inhibits iron metabolism and suppresses lung cancer through activation of P53-miR-34a-E2F1/E2F3 pathway. *Sci. Rep.* **7**, 1–12 (2017).
30. Niculescu, A. B. III. *et al.* Effects of p21Cip1/Waf1 at both the G1/S and the G2/M cell cycle transitions: pRb is a critical determinant in blocking DNA replication and in preventing endoreduplication. *Mol. Cell. Biol.* **18**, 629–643 (1998).
31. Nachmias, B. & Schimmer, A. D. Targeting nuclear import and export in hematological malignancies. *Leukemia* **34**, 2875–2886 (2020).
32. Miles, X., Vandevoorde, C., Hunter, A. & Bolcaen, J. MDM2/X inhibitors as radiosensitizers for glioblastoma targeted therapy. *Front. Oncol.* **11**, 703442 (2021).
33. Spencer, S. L. *et al.* The proliferation-quiescence decision is controlled by a bifurcation in CDK2 activity at mitotic exit. *Cell* **155**, 369–383 (2013).
34. Dong, P., Zhang, C., Parker, B.-T., You, L. & Mathey-Prevot, B. Cyclin D/CDK4/6 activity controls G1 length in mammalian cells. *PLoS ONE* **13**, e0185637 (2018).
35. Gu, Y. *et al.* MCM6 indicates adverse tumor features and poor outcomes and promotes G1/S cell cycle progression in neuroblastoma. *BMC Cancer* **21**, 1–14 (2021).
36. Jia, W. *et al.* The impact of MCM6 on hepatocellular carcinoma in a Southern Chinese Zhuang population. *Biomed. Pharmacother.* **127**, 110171 (2020).
37. Vigouroux, C. *et al.* Methyl (R217) HuR and MCM6 are inversely correlated and are prognostic markers in non small cell lung carcinoma. *Lung Cancer* **89**, 189–196 (2015).
38. Kwok, H. F. *et al.* Prognostic significance of minichromosome maintenance proteins in breast cancer. *Am. J. Cancer Res.* **5**, 52 (2015).
39. Malinowski, D. P. Molecular diagnostic assays for cervical neoplasia: Emerging markers for the detection of high-grade cervical disease. *Biotechniques* **38**, S17–S23 (2005).
40. Mathews, C. K. Deoxyribonucleotide metabolism, mutagenesis and cancer. *Nat. Rev. Cancer* **15**, 528–539 (2015).
41. Zhang, H. *et al.* Effect of CCNB1 silencing on cell cycle, senescence, and apoptosis through the p53 signaling pathway in pancreatic cancer. *J. Cell. Physiol.* **234**, 619–631 (2019).
42. Pucci, B., Kasten, M. & Giordano, A. Cell cycle and apoptosis. *Neoplasia* **2**, 291–299 (2000).
43. Li, B. *et al.* Regulating the CCNB1 gene can affect cell proliferation and apoptosis in pituitary adenomas and activate epithelial-to-mesenchymal transition. *Oncol. Lett.* **18**, 4651–4658 (2019).
44. Li, M., Shang, H., Wang, T., Yang, S.-Q. & Li, L. Huanglian decoction suppresses the growth of hepatocellular carcinoma cells by reducing CCNB1 expression. *World J. Gastroenterol.* **27**, 939 (2021).
45. Zilfou, J. T. & Lowe, S. W. Tumor suppressive functions of p53. *Cold Spring Harb. Perspect. Biol.* **1**, a001883 (2009).
46. Cao, L., Li, W., Kim, S., Brodie, S. G. & Deng, C.-X. Senescence, aging, and malignant transformation mediated by p53 in mice lacking the Brca1 full-length isoform. *Genes Dev.* **17**, 201–213 (2003).
47. Lakin, N. D. & Jackson, S. P. Regulation of p53 in response to DNA damage. *Oncogene* **18**, 7644–7655 (1999).
48. Giono, L. E. & Manfredi, J. J. The p53 tumor suppressor participates in multiple cell cycle checkpoints. *J. Cell. Physiol.* **209**, 13–20 (2006).
49. Biegging, K. T., Mello, S. S. & Attardi, L. D. Unravelling mechanisms of p53-mediated tumour suppression. *Nat. Rev. Cancer* **14**, 359–370 (2014).
50. Li, S., Zhang, W., Chen, B., Jiang, T. & Wang, Z. Prognostic and predictive value of p53 in low MGMT expressing glioblastoma treated with surgery, radiation and adjuvant temozolomide chemotherapy. *Neurol. Res.* **32**, 690–694 (2010).
51. Afshar, G. *et al.* Radiation-induced caspase-8 mediates p53-independent apoptosis in glioma cells. *Cancer Res.* **66**, 4223–4232 (2006).
52. Cerrato, J. A., Yung, W. A. & Liu, T.-J. Introduction of mutant p53 into a wild-type p53-expressing glioma cell line confers sensitivity to Ad-p53-induced apoptosis. *Neuro Oncol.* **3**, 113–122 (2001).
53. Voloshin, T. *et al.* Tumor treating fields (TTFields) hinder cancer cell motility through regulation of microtubule and actin dynamics. *Cancers* **12**, 3016 (2020).
54. Landry, M., Nelson, D., Choi, E., DuRoss, A. & Sun, C. Development of a G2/M arrest high-throughput screening method identifies potent radiosensitizers. *Transl. Oncol.* **16**, 101336 (2022).

Author contributions

R.M., A.M.A., and F.Sh. performed the laboratory experiments and drafted the first version of the M.A.S.; A.M.A., F.F., S.P.Sh., and A.S. helped with data analysis; M.A.J., S.P.Sh., and A.M.A. conceived the main idea of the study; M.A.J. supervised the team.

Competing interests

The authors declare no competing interests.

Additional information

Correspondence and requests for materials should be addressed to M.A.J.

Reprints and permissions information is available at www.nature.com/reprints.

Publisher's note Springer Nature remains neutral with regard to jurisdictional claims in published maps and institutional affiliations.



Open Access This article is licensed under a Creative Commons Attribution 4.0 International License, which permits use, sharing, adaptation, distribution and reproduction in any medium or format, as long as you give appropriate credit to the original author(s) and the source, provide a link to the Creative Commons licence, and indicate if changes were made. The images or other third party material in this article are included in the article's Creative Commons licence, unless indicated otherwise in a credit line to the material. If material is not included in the article's Creative Commons licence and your intended use is not permitted by statutory regulation or exceeds the permitted use, you will need to obtain permission directly from the copyright holder. To view a copy of this licence, visit <http://creativecommons.org/licenses/by/4.0/>.

© The Author(s) 2023